LETTERS
PUBLISHED ONLINE: 25 NOVEMBER 2012 | DOI: 10.1038/NNANO.2012.208
nature nanotechnology

# A sub-1-volt nanoelectromechanical switching device

Jeong Oen Lee[1], Yong-Ha Song[1], Min-Wu Kim[1], Min-Ho Kang[2], Jae-Sub Oh[2], Hyun-Ho Yang[1] and Jun-Bo Yoon[1]*

**Nanoelectromechanical (NEM) switches[1–6] have received widespread attention as promising candidates in the drive to surmount the physical limitations currently faced by complementary metal oxide semiconductor technology. The NEM switch has demonstrated superior characteristics including quasi-zero leakage behaviour[1], excellent density capability[2] and operation in harsh environments[3]. However, an unacceptably high operating voltage (4–20 V) has posed a major obstacle in the practical use of the NEM switch in low-power integrated circuits. To utilize the NEM switch widely as a core device component in ultralow power applications[7–11], the operation voltage needs to be reduced to 1 V or below. However, sub-1 V actuation has not yet been demonstrated because of fabrication difficulties and irreversible switching failure caused by surface adhesion. Here, we report the sub-1 V operation of a NEM switch through the introduction of a novel pipe clip device structure and an effective air gap fabrication technique. This achievement is primarily attributed to the incorporation of a 4-nm-thick air gap, which is the smallest reported so far for a NEM switch generated using a 'top-down' approach. Our structure and process can potentially be utilized in various nanogap-related applications, including NEM switch-based ultralow-power integrated circuits, NEM resonators[12,13], nanogap electrodes for scientific research[14] and sensors[15].**

A typical NEM switch[3,5,6] makes use of a plane capacitor structure (metal–air–metal) with a cantilever or clamped beam structure[16]. To achieve low-voltage operation in this structure, a design modification that reduces the entire thickness of the air gap is considered to be the most effective scaling mechanism[17]. However, when electrostatic force is applied, the top electrode collapses down to the bottom electrode with zipping actuation, and the contact area increases, which allows the surface attraction force to dominate the restoring force so that permanent adhesion occurs. Therefore, achieving reversible operation with sub-1 V actuation is considered one of the most important challenges to overcome[18]. We propose an effective 'pipe clip' structure (Fig. 1a) that introduces an extremely small air gap (<10 nm) in only part of the electrode so as to obtain a sub-1 V operating voltage. The proposed device has a two-terminal configuration consisting of a fixed bottom electrode and a freely suspended electrode, similar to the shape of a square pipe clip. Note that although the traditional plane structure (upper panel in Fig. 1b) has a homogeneous air gap between the electrodes, the proposed pipe clip structure (lower panel in Fig. 1b) also contains extremely small air gaps on the side edges of the bottom electrode and a restricted contact area so as to reduce the van der Waals force that is responsible for permanent adhesion failure. The mechanical separation between the suspended and bottom electrodes completely prevents leakage current at the OFF state. When we apply enough voltage between these two electrodes, the suspended electrode collapses down to the bottom electrode because of the 'pull-in' phenomenon, which establishes a mechanical contact and creates a current path at the ON state. Although this concept is not appropriate for high-power radiofrequency applications because of self-actuation[19], it can be applied to cross-bar memory devices[2,5,20] or a transformable building block[21] as possible (primitive) solutions for integrated circuit applications that favour two-terminal configurations. Also, if we exploit the pipe clip structure more than once, in both an actuation part and a conducting part, the device can be extended to a three-terminal configuration, which is to be developed further in the near future.

Because the electric field plays a significant role in achieving electrostatic force, the magnitude and distribution of the electric field inside the proposed structure must be estimated. The electric field gradient can be obtained from a two-dimensional simulation, as shown by the colour-coded contour in Fig. 1b. The average magnitude of the electric field in the flat regions of both the plane structure and the pipe clip structure is only 15 MV $m^{-1}$ (separation gap, 30 nm), whereas the maximum electric field in the narrow regions of the pipe clip structure (separation gap, 4 nm) is 99 MV $m^{-1}$. The calculated electrostatic force in the pipe clip structure is considered to be at least 10 times greater than that of the plane structure when it is assumed that the minimum air gap is significantly smaller than the length or width of the electrode. These results indicate that the fabrication of an extremely small air gap will be primarily responsible for determining the electrostatic force and operation voltage, regardless of the area of the electrode.

Several effective and creative methods for fabricating nanogap electrodes with controlled spacing have been investigated using approaches[22] including electron beam lithography (EBL), electromigration[23] or the electroplating method[24]. In the electromigration method, the nanosized gap is formed at the point at which an excessive current flow breaks the electrode, and in the electroplating method, the gap is narrowed by depositing material on the side wall of the pre-defined air gap. Because these processes provide only one thickness of air gap for the fixed electrodes, they cannot be used to form a 'pipe-clip' structure, which requires a dual thickness for the air gap and a movable electrode. We proposed an effective fabrication technique using a pre-patterned trench structure (referred to as a 'self-aligned trench', Fig. 1c) that builds the 'pipe-clip structure' by means of simple fabrication steps (see Methods) motivated by spacer lithography[25]. Figure 1d shows schematics of the process. The thickness of the spacer on the side edges can be optimized by increasing the depth of the trench or changing the

[1]Department of Electrical Engineering, Korea Advanced Institute of Science and Technology (KAIST), 291 Daehak-ro, Yuseong-gu, Daejeon, 305-701, Republic of Korea, [2]Korea National NanoFab Center (NNFC), 291 Daehak-ro, Yuseong-gu, Daejeon, 305-701, Republic of Korea.
*e-mail: jbyoon@ee.kaist.ac.kr

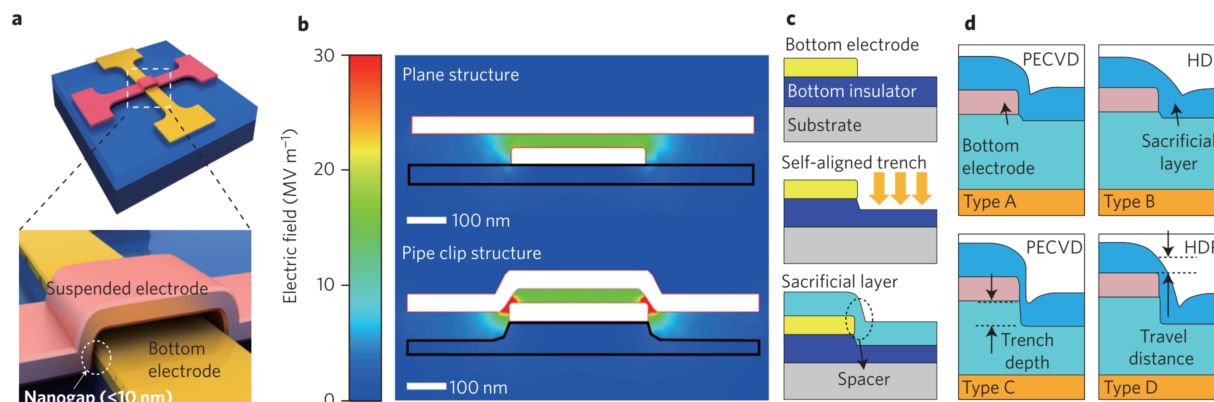


**Figure 1 | Structure of the NEM switch and operation scheme.** **a**, Schematic of the two-terminal NEM switch with the pipe clip structure. An extremely small nanogap (<10 nm) is built in the side edges of the bottom electrode. **b**, Electric field distribution of the traditional plane structure (upper) and the proposed pipe clip structure (lower). **c**, Fabrication process for the self-aligned trench technique introducing the ultrathin spacer structure, which in turn forms an extremely small air gap in the proposed pipe clip structure. **d**, Simulation results for optimizing the spacer profile. Types A and B show the sacrificial layer profile on a shallow trench structure, and types C and D show the sacrificial layer profile on a deep trench structure. Types A and C are simulated results from the PECVD deposition. Types B and D correspond to HDP deposition.

deposition method. The plasma-enhanced chemical vapour deposition (PECVD) method yields a bumpy profile of the sacrificial layer at the top corner of the bottom electrode, which is imperfect as a contact structure (types A and C in Fig. 1d). However, the high density plasma (HDP)[28] method provides a more favourable structure with rounded edges (types B and D).

Figure 2a presents schematics of the plane and pipe clip structures. Corresponding scanning electron microscopy (SEM) images of the fabricated devices are shown in Fig. 2b. In this test experiment, a sacrificial layer with a thickness of 50 nm was prepared to generate a sufficiently large air gap to facilitate an operating voltage difference derived from the contribution of the pipe clip structure. Figure 2c shows the measured $I$–$V$ curves from the two types of 2-μm-long devices. Below the operating voltage (sub-pull-in region), the $I$–$V$ curve shows an insignificant leakage current. With increasing applied voltage, the current curve rises steeply (transition region) from a non-conducting state (~100 fA) to a conducting state (100 nA) at a voltage that corresponds to the operation point of each device. The on/off current ratio exceeded $1 \times 10^6$. To evaluate a possible tunnelling effect in the pipe clip structure, we performed a Fowler–Nordheim (F–N) analysis (Supplementary Section G). This analysis suggested that the tunnelling current is insignificant in the sub-pull-in region. Although the tunnelling effect can be involved in $I$–$V$ behaviour when the air gap is reduced to 2 nm and a large voltage is applied (>10 V), the measured F–N slope parameter $S$ (−1,288) in the transition region still cannot be explained by the tunnelling model without considering mechanical motion. We believe that a relatively small contact force (380 nN, see Methods) and contaminations on the contact surface are mainly responsible for the non-ideal transition current behaviour (unstable fluctuation or gradual increase in the transition region), because similar $I$–$V$ behaviour has been observed in various nano- or micro-electromechanical (NEM/MEM) switches when the contact force was relatively low or dielectric contaminations (for example, hydrocarbon or native metal oxide) were observed on the contact surface.

The electromechanical characteristic of the pipe clip structure was evaluated from a three-dimensional finite-element simulation. Figure 2d shows the electrostatic pressure (force per unit area) distribution on the surface of the pipe clip structure when 1 V is applied between the electrodes. A large amount of electrostatic pressure is exerted at the corners of the bottom electrode because of the minimum separation distance there and the quadratic behaviour of the electrostatic force. Inspired by the simulation result, we simplified the pipe clip structure using the lumped model presented in the inset of Fig. 2e (Supplementary Fig. S1). The electrostatic force in the minimum gap region $g_s$ and the flat gap region $g_f$ was calculated as $F_s$ (solid red line) and $F_f$ (dashed black line), respectively. The red asterisks (pipe clip) and black crosses (plane) correspond to the total electrostatic force extracted from the three-dimensional finite-element simulation.

Figure 2f shows the electrostatic pull-in voltage as a function of device length, $L$. The black squares and red circles correspond to the measured operating voltage sets from the plane beam structure and the pipe clip structure, respectively. The black and red dashed lines represent the theoretically predicted values calculated from the simplified model for the plane and pipe clip beam structures, respectively. A significant reduction of the operating voltage (73% for a length of 1.5 μm) was observed in the pipe clip structure compared with the plane structure, although the area of the extremely small air gap occupies only 4% of the actuating electrode. The black crosses and red asterisks represent the pull-in voltages obtained from the three-dimensional finite-element simulation. The consistency between the results of the analytical model and the three-dimensional finite-element simulation implies that the simplified analytical model is well suited to describing the electromechanical behaviour of the three-dimensional pipe clip beam structure, which leads us to consider that the electrostatic force in the minimum gap region is mainly responsible for the electromechanical behaviour of the pipe clip structure. The agreement between the measured data and the predicted values indicates that the proposed approach provides an adoptable design-to-fabrication consistency. In this test experiment, the effect of the pipe clip structure (reduction of the operating voltage) was verified, although the operating voltage did not reach the sub-1 V order. To further reduce the operating voltage, another NEM switch was fabricated using a 30-nm-thick sacrificial layer. A cross-sectional transmission electron microscope (TEM) image of the fabricated device is shown in Fig. 3a. The length and width of the suspended electrode are 1,400 nm and 300 nm, respectively. After removing the sacrificial layer, the thickness of the extremely small air gap formed on the side edges of the bottom electrode was evaluated using a TEM, as shown in Fig. 3b. The thickness of the obtained air gap is ~4 nm, which is the smallest reported to date for a NEM switch. This result is attributed to the proposed fabrication technique for the sacrificial layer, which is formed by using the HDP deposition method on the self-aligned trench.

 NATURE NANOTECHNOLOGY DOI: 10.1038/NNANO.2012.208

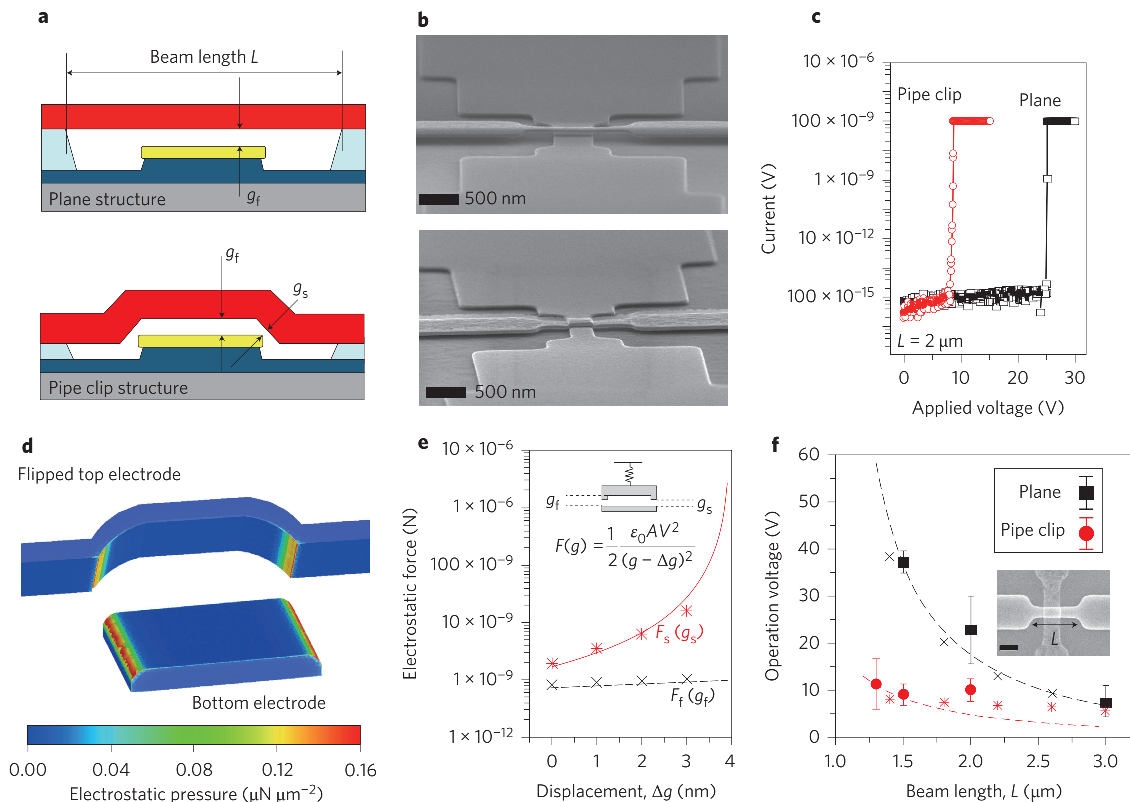


**Figure 2 | Comparison of operating voltage for plane and pipe clip structures. a**, Schematic of the plane and pipe clip structures. **b**, Related SEM images after fabrication (total length of beam $L = 1.3$–$3.0$ μm; thickness of the larger gap $g_f = 50$ nm; thickness of the smaller gap $g_s = 10$ nm). **c**, Measured current versus voltage curve. **d**, Finite-element method (FEM) simulation for electrostatic pressure (electrostatic force per unit area) for the pipe clip structure. **e**, Total electrostatic force as a function of displacement. The red solid line is obtained from the simplified lumped model for the pipe clip structure, and the black dashed line is the calculated electrostatic force from the plane beam model. The red asterisks and black crosses are obtained from the FEM simulation for the pipe clip and plane structures, respectively. **f**, Operating voltage (electrostatic pull-in voltage) as a function of beam length. Black solid squares show the measured pull-in voltages and the black dashed line the estimated values from a lumped model for the plane structure. Black crosses denote the pull-in voltage obtained from the FEM simulation for the plane structure. The red solid circles and red dashed line correspond to the measured pull-in voltage and lumped model data for the pipe clip structure, respectively. Red asterisks denote the pull-in voltage obtained from the FEM simulation for the pipe clip structure. Error bars indicate the standard error between individual samples.

The electrical characterization of the fabricated device is presented in Fig. 4a. The voltage on the $x$-axis denotes the applied voltage across the beam and the bottom electrode, and the current on the $y$-axis indicates the current flow between the two electrodes. The device performed a switching operation at ~400 mV, a low voltage for actuating NEM devices. At the sub-pull-in region, we observed a pico-ampere level of current flow. Note that the same current behaviour was observed from a probing pad pattern (Supplementary Section F). It is therefore reasonable to conclude that the sub-pull-in current is only associated with probing pads such as pad-to-pad or pad-to-substrate leakages. The same sub-pull-in current behaviour between the device pattern and the probing pad pattern indicates the rare possibility of a tunnelling effect in the sub-pull-in region and clear isolation of the nanogap placed between the bottom electrode and the suspended top electrode in the initial state. The device also showed an abrupt switching characteristic: the sub-threshold slope was less than 10 mV/dec, which is far lower than the theoretical limitation (60 mV/dec) of complementary metal–oxide semiconductor (CMOS) devices at room temperature. The calculated current density through the suspended electrode was 833 A cm$^{-2}$. The on/off current ratio exceeded $1 \times 10^5$. Figure 4b presents the $I$–$V$ characteristics during the cyclic measurements. The current curve, which repeatedly rises at the same voltage during cyclic testing, suggests the occurrence of mechanical actuation induced by the electrostatic force. The unstable current characteristic for the transition state can be interpreted as the physical degradation of the contact surface, which is consistent with previous results[29,30] obtained for various NEM switches. Although the device showed poor reliability, it is encouraging to note that some results involving the

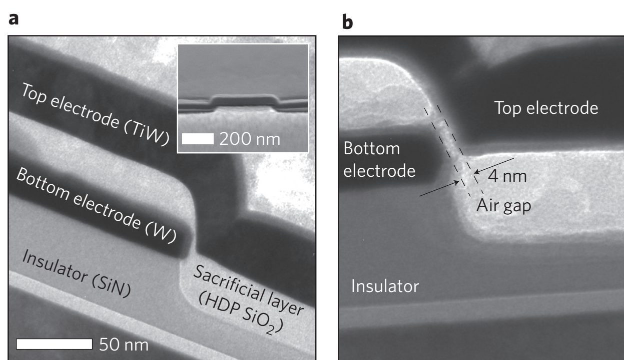


**Figure 3 | The fabricated two-terminal NEM switch. a**, TEM image of the device before removing the sacrificial layer (total beam length $L = 1{,}400$ nm; beam width $W = 300$ nm; beam thickness = 40 nm; width of bottom electrode $D = 500$ nm). **b**, Magnified cross-sectional TEM image of the contact point with a 4-nm-thick air gap after removing the sacrificial layer.

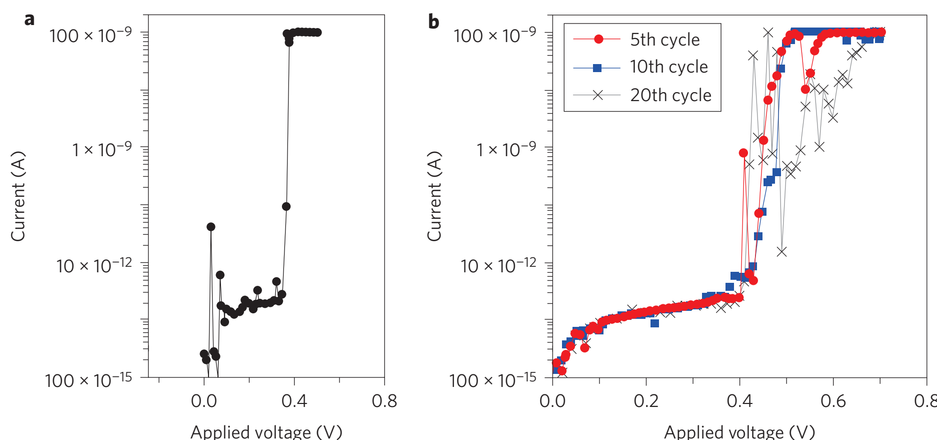


**Figure 4 | *I–V* characteristics of the two-terminal NEM switch. a**, The *I–V* characteristics show a two-terminal switch behaviour. The current curve rises abruptly at an applied voltage of 400 mV. Below the turn-on voltage, the current shows the noise floor of the measurement equipment. **b**, *I–V* characteristic during several cyclic measurements. The conducting state is unstable; consequently, the current level of the ON state rapidly degrades as the number of contacts increases. However, the operating voltage (400 mV) was sustained during the cyclic test.

introduction of an $SiO_2$ layer on the contacting surface[5] or the adoption of SiC[3] as a device material may suggest the possible development of a highly reliable NEM switch in the near future. We expect that the use of noble metals (for example, Ru, Ir and Pt), which are resistant to corrosion and contamination, will lead to further improvements in reliability. In our present version of the device, we observed unwanted titanium oxide or tungsten oxide on the surfaces of the fabricated electrodes (by TEM and X-ray photoelectron spectroscopy (XPS) analysis). We suggest that the elimination of metal oxide by introducing non-oxygen deposition process (for example, polysilicon or another sacrificial layer that does not react with the metal electrodes) will effectively improve contact reliability. To exploit various materials in the proposed device structure, it will be effective to use an atomic layer deposition technique, which allows the deposition of layers as fine as ~0.1 Å per cycle.

In conclusion, we have demonstrated a sub-1 V operating voltage for the first time in a NEM switch. Three key features of the pipe clip structure contributed to overcoming the fabrication difficulties and conflicting requirements for low-voltage operation: (i) an extremely small air gap (4 nm); (ii) a unique contact structure to decrease the adhesion force; and (iii) a simple fabrication technique using a self-aligned trench structure. This procedure is well suited for use in NEM–CMOS hybrid integrated circuits designed for ultra-low-power applications. The fabrication technique is also applicable to various NEM devices, sensors and nanogap electrodes.

## Methods

**Self-aligned trench formation.** The bottom electrode was intentionally over-etched into the substrate, using the bottom electrode as a self-aligned etch mask. An $SiO_2$ film deposited on the pre-patterned trench then formed the spacer structure[26], the thickness of which on the side edge of the bottom electrode was much less than that of the film formed on top of the trench. The top electrode was subsequently formed on the $SiO_2$ spacer structure, which was later removed to create an air gap between the top and bottom electrodes (the profile of the air gap therefore being identical to that of the spacer structure). We found that the depth of the trench and the deposition method are major tuning parameters for determining the profile of the sacrificial layer, which, in turn, determines the air gap structure (Supplementary Sections C and D). The proposed process can provide an extremely smooth surface on the side wall of the trench due to the planarization effect of the etching process[27].

**Calculation of mechanical performance.** We assumed that the suspended pipe clip structure and the bottom electrode behave as two parallel plates. The spring constant of the suspended beam was estimated using the equation $k = 59.52Ew(t/l)^3$, where $E$ is Young's modulus (450 GPa), $t$ is the thickness of the beam, $l$ is the length, and $w$ is the width of the beam. The resonance frequency was derived from

$$\frac{f}{2\pi} = \sqrt{\frac{k}{m}} = 1.03\sqrt{\frac{E}{\rho}\frac{t}{L^2}}$$

where $\rho$ is the density of TiW (142,000 kg m$^{-3}$). The switching speed is calculated from

$$t_s \cong 3.67\frac{V_p}{V_s\omega_0}$$

where the operation voltage $V_p$ is 0.4 V and the applied voltage $V_s$ is 1 V. The natural oscillating frequency[13] of the suspended electrode can be estimated as 3.74 MHz by calculation, which corresponds to a switching speed of 62.5 ns. The calculated spring constant for the spring structure and the restoring force are 54 N m$^{-1}$ and 380 nN, respectively.

Received 4 July 2012; accepted 24 October 2012; published online 25 November 2012

## References

1. Jang, J. E. *et al.* Nanoscale memory cell based on a nanoelectromechanical switched capacitor. *Nature Nanotech.* **3,** 26–30 (2008).
2. Rueckes, T. *et al.* Carbon nanotube-based nonvolatile random access memory for molecular computing. *Science* **289,** 94–97 (2000).
3. Lee, T-H., Bhunia, S. & Mehregany, M. Electromechanical computing at 500 °C with silicon carbide. *Science* **329,** 1316–1318 (2010).
4. Lee, S. W. *et al.* A three-terminal carbon nanorelay. *Nano. Lett.* **4,** 2027–2030 (2004).
5. Jang, W. W. *et al.* Fabrication and characterization of a nanoelectromechanical switch with 15-nm-thick suspension air gap. *Appl. Phys. Lett.* **92,** 103110 (2008).
6. Lee, S. W., Park, S. J., Campbell, E. E. B. & Park, Y. W. A fast and low-power microelectromechanical system-based non-volatile memory device. *Nature Commun.* **2,** 220 (2010).
7. Raghunathan, V., Kansal, A., Hsu, J., Friedman, J. & Srivastava, M. Design considerations for solar energy harvesting wireless embedded systems. *Proc. IPSN*, 457–462 (2005).
8. Service, R. F. Nanogenerators tap waste energy to power ultrasmall electronics. *Science* **328,** 304–305 (2010).
9. Xu, S. *et al.* Self-powered nanowire devices. *Nature Nanotech.* **5,** 366–373 (2010).
10. Tian, B. Z. *et al.* Coaxial silicon nanowires as solar cells and nanoelectronic power sources. *Nature* **449,** 885–890 (2007).
11. Yang, R., Qin, Y., Dai, L. & Wang, Z. L. Power generation with laterally packaged piezoelectric fine wires. *Nature Nanotech.* **4,** 34–39 (2009).
12. Naik, A. K., Hanay, M. S., Hiebert, W. K., Feng, X. L. & Roukes, M. L. Towards single-molecule nanomechanical mass spectrometry. *Nature Nanotech.* **4,** 445–450 (2009).
13. Ekinci, K. L. & Roukes, M. L. Nanoelectromechanical systems. *Rev. Sci. Instrum.* **76,** 061101 (2005).
14. Ward, D. R., Hűser, F., Pauly, F., Cuevas, J. C. & Natelson, D. Optical rectification and field enhancement in a plasmonic nanogap. *Nature Nanotech.* **5,** 732–736 (2010).
15. Im, H., Huang, X-J., Gu, B. & Choi, Y-K. A dielectric-modulated field-effect transistor for biosensing. *Nature Nanotech.* **2,** 430–434 (2007).
16. Rebeiz, G. M. *RF MEMS: Theory, Design and Technology* (Wiley, 2003).
17. Akarvardar, K. *et al.* Design considerations for complementary nanoelectromechanical logic gates. *IEEE IEDM Tech. Digest*, 299–302 (2007).

18. Loh, O. Y. & Espinosa, H. D. Nanoelectromechanical contact switches. *Nature Nanotech.* **7,** 283–295 (2012).
19. Dussopt, L. & Rebeiz, G. M. Intermodulation distortion and power handling in RF MEMS switches, varactors and tunable filters. *IEEE Trans. Microw. Theory Tech.* **51,** 1247–1256 (2003).
20. Choi, W. Y., Kam, H., Lee, D., Lai, J. & King, T-J. Compact nanoelectro-mechanical non-volatile memory (NEMory) for 3D integration. *IEEE IEDM Tech. Digest*, 603–606 (2007).
21. Choi, S-J. *et al.* Transformable functional nanoscale building blocks with wafer-scale silicon nanowires. *Nano Lett.* **11,** 854–859 (2011).
22. Li, B. T., Hu, W. & Zhu, D. Nanogap electrodes. *Adv. Mater.* **22,** 286–300 (2010).
23. Johnston, D. E., Strachan, D. R. & Johnson, A. T. C. Parallel fabrication of nanogap electrodes. *Nano Lett.* **7,** 2774–2777 (2007).
24. Yasutake, Y. *et al.* Simultaneous fabrication of nanogap gold electrodes by electroless gold plating using a common medical liquid. *Appl. Phys. Lett.* **91,** 203107 (2007).
25. Choi, Y-K., King, T-J. & Hu, C. Nanoscale CMOS spacer FinFET for the terabit era. *IEEE Electron. Dev. Lett.* **23,** 25–27 (2002).
26. Horstmann, J. T., Hilleringmnn, U. & Goser, K. F. Matching analysis of deposition defined 50-nm MOSFET. *IEEE Trans. Electron. Dev.* **45,** 299–306 (1998).
27. Stern, E. *et al.* Label-free immunodetection with CMOS-compatible semiconducting nanowires. *Nature* **445,** 519–522 (2007).
28. Mungekar, H. P. & Lee, Y. S. High density plasma chemical vapor deposition gap-fill mechanisms. *J. Vac. Sci. Technol. B* **24,** L11 (2006).
29. Davidson, B. D., Seghete, D., George, S. M. & Bright, V. M. ALD tungsten NEMS switches and tunneling devices. *Sens. Actuat. A* **166,** 269–276 (2011).
30. Lee, J. O. *et al.* 3-terminal nanoelectromechanical switching device in insulating liquid media for low voltage operation and reliability improvement. *IEEE IEDM Tech. Digest*, 227–230 (2009).

## Acknowledgements

This work was supported by the Smart IT Convergence System Research Center, which is funded by the Ministry of Education, Science and Technology as a Global Frontier Project, and also partially supported by the National Research Foundation of Korea (NRF) grant funded by the Korea government (MEST) (no. 20120000823). The authors would like to thank Yang-Kyu Choi for experimental support.

## Author contributions

J.O.L. conceived the idea and performed experimental work and data analysis. M-H.K. and J-S.O. contributed to the fabrication process. J.O.L., M-W.K. and Y-H.S. performed modelling and interpretation. H-H.Y. participated in data analysis. J-B.Y. inspired the research, with guidance, and participated in data analysis. The manuscript was written by J.O.L. and J-B.Y. All authors discussed the results and commented on the manuscript.

## Additional information

Supplementary information is available in the online version of the paper. Reprints and permission information is available online at http://www.nature.com/reprints. Correspondence and requests for materials should be addressed to J.B.Y.

## Competing financial interests

The authors declare no competing financial interests.